Clin. Lab. 2026;72:XXX-XXX

ORIGINAL ARTICLE

Development and Validation of a Cuproptosis-Related Gene Signature for Prognostic Stratification in Papillary Renal Cell Carcinoma

Haixia Li [1], Li Cao [2], Ruimin Li [2], Ling Xu [2], Shuxia Zhang [2], Jianjun Gao [2], Yongxue Chen [1], Xiaoqiang Lian [2]

[1] *Anesthesiology Department, Handan Central Hospital, Handan, China*
[2] *Department of Clinical Laboratory, Handan Central Hospital, Handan, China*

SUMMARY

Background: **Cuproptosis is defined as a novel form of regulated cell death triggered by copper accumulation, with emerging evidence linking cuproptosis-related genes (CRGs) to tumor progression. However, the prognostic relevance of CRGs in papillary renal cell carcinoma (PRCC) remains elusive. This study aimed to construct and validate a cuproptosis-related gene prognostic signature for PRCC, and to explore its potential value in risk stratification, immune infiltration, and pathogenesis.**

Methods: **Transcriptomic profiles and clinical data were sourced from the Cancer Genome Atlas Program. Univariate Cox regression assessed the prognostic potential of 17 CRGs, while Lasso-penalized Cox regression identified risk genes for signature construction. Kaplan-Meier curves illustrated survival probabilities, and receiver operating characteristic curves were drawn to evaluate signature predictive performance. External validation was performed using data from the Gene Expression Omnibus. Biological functions were explored through Gene Ontology (GO) and Kyoto Encyclopedia of Genes and Genomes (KEGG) enrichment analyses, with validation via gene set variation analysis (GSVA). Immune cell infiltration was assessed using QuanTIseq algorithm.**

Results: **The PRCC cohort from The Cancer Genome Atlas Program (TCGA) was randomly split into training (n = 183) and validation (n = 75) sets, with GSE2748 (n = 29) from GEO for external validation. Univariate Cox analysis identified 7 CRGs as prognostic factors in PRCC. A risk signature comprising 5 CRGs (DLST, PDHB, SLC25A3, ATP7A, and GLS) was developed using Lasso-penalized Cox regression. Kaplan-Meier curves indicated lower survival probabilities in patients with higher risk scores. ROC analysis demonstrated the cuproptosis risk signature's strong performance for overall survival at 1, 3, and 5 years. GO and KEGG analyses revealed that metabolic processes were the predominant pathways enriched in DEGs between high- and low-risk groups, a finding further validated by GSVA. Immune infiltration analysis highlighted macrophages and neutrophils as the dominant immune cells, with significantly higher Tregs observed in the tumor microenvironment of high-risk patients ($p < 0.05$).**

Conclusions: **This study presents a novel five-gene prognostic signature for PRCC based on 17 CRGs, offering promising performance in risk stratification and providing insights into PRCC pathogenesis, particularly in cellular metabolism.**

(Clin. Lab. 2026;72:xx-xx. DOI: 10.7754/Clin.Lab.2025.250554)

Correspondence:
Xiaoqiang Lian
Department of Clinical Laboratory
Handan Central Hospital
No. 15, South Zhonghua Street
Handan City
China
Phone: + 86 03102118530
Email: lalmail@126.com

KEYWORDS

papillary renal cell carcinoma, cuproptosis, risk signature, metabolism, immune infiltration cells

Manuscript accepted July 14, 2025

INTRODUCTION

Renal carcinoma (RCC) is a group of heterogeneous diseases with various clinical, histological and genetic features. Globally, the incidence and mortality rates of RCC have been increasing over the years. In 2012, approximately 348,000 patients were newly diagnosed with RCC, and 143,000 died of this disease [1]. However, the number of new cases increased to 400,000, along with 175,000 deaths due to RCC in 2018 [2]. To date, RCC has become one of the most common tumors in the world, although the incidence is slightly lower in females [3]. Papillary renal cell carcinoma (PRCC), accounting for 15% - 20% of all cases [4,5], represents the second most predominant subtype of RCC. Histologically, PRCC is typically characterized by papillary structures and a higher rate of multifocal lesions. PRCC is mainly divided into two major subtypes based on distinct papillary structures [5]. Type 1 consists of a single layer of papillary epithelial cells composed of cuboidal or columnar epithelial cells with little cytoplasm, small ovoid nuclei with tiny nucleoli; in contrast, tumor cells of Type 2 PRCC have abundant eosinophilic cytoplasm, large spherical nuclei with prominent nucleoli. While favorable outcomes are generally determined by active treatment [6], patients with PRCC exhibit relatively worse outcomes than those with clear cell renal cell carcinoma (ccRCC) when metastasis or progression occurs [7].

The development of high-throughput sequencing has contributed to a panoramic view of tumor molecular profiles. Different molecular patterns in tumors may be strongly correlated with prognosis. Previous studies have confirmed that activated ferroptosis, triggered by the iron-dependent accumulation of oxidized lipids, could inhibit the cell proliferation of RCC [8]. Based on immune-related genes, Wang et al. developed a robust risk signature and were able to independently predict outcomes for PRCC patients [9]. Furthermore, a three-gene prognostic model associated with cell cycle, nucleotide repair, and purine metabolism also suggested a favorable prediction performance in the prognosis of PRCC [10]. Recently, cuproptosis was defined as a new type of regulated cell death induced by cellular copper accumulation [11]. Unlike other regulated cell deaths, cuproptosis mainly involves mitochondrial damage: when copper binds to the lipoylated component of the tricarboxylic acid cycle, the excessive accumulation of conjugates and the subsequent loss of Fe-S cluster protein can trigger a series of proteotoxic stress reactions that ultimately lead to cell death [11]. Programmed cell death is generally associated with tumorigenesis, progression, and even metastasis.

A study has revealed a potential link between cuproptosis and the prognosis of ccRCC, which provides new insight into therapy [12]. In this study, we identified the expression of CRGs in the PRCC cohort from the Cancer Genome Atlas Program (TCGA), an open-access database providing molecular profiles of various cancers. A five-gene risk signature was constructed using Lasso-penalized Cox regression, with subsequent validation in an internal validation set. The PRCC dataset from the Gene Expression Omnibus (GEO) was used for external validation. We further analyzed differences in biological functions and immune cell infiltration between patients with high and low risk scores to explore the underlying mechanisms.

MATERIALS AND METHODS

Data acquisition and preprocessing

The RNA sequencing (RNA-seq) data and corresponding clinical information of PRCC were retrieved from the Kidney Renal Papillary Cell Carcinoma cohort in the TCGA (https://portal.gdc.cancer.gov/). Essential clinical characteristics included age, gender, stage, survival status, and overall survival time. Patients were excluded if they had incomplete clinical data or a survival time of < 30 days. Then, we randomly split the patients into a training set and a validation set at a 7:3 ratio using the "caret" R package. The microarray data (GSE2748) from GEO (https://www.ncbi.nlm.nih.gov/geo/) was used for external validation.

A total of 17 CRGs, including FDX1 (a reductase that reduces $Cu2^+$ to Cu^+), SLC31A1, SLC25A3, ATP7B and ATP7A for copper transportation, and other related genes MTF1, GLS, CDKN2A, LIPT1, LIAS, DLD, DLAT, PDHA1, PDHB, DBT, GCSH, and DLST were collected from several cuproptosis-related studies [11-1312]. Differential expression analysis was performed between tumors and adjacent normal tissues using the "limma" R package. Differential expression was defined as $|\log2 \text{ (fold change)}| > 0.75$ and adjusted p-value < 0.05. To explore the relationship between cuproptosis and outcome in PRCC, univariate Cox analysis was performed on 17 CRGs for overall survival using the "survival" R package.

Cuproptosis-related risk signature construction by dimension reduction analysis

In this study, we considered overall survival as the end point of the risk signature. Lasso-penalized Cox regression with 10-fold cross-validation was performed on 17 CRGs in the training set using the "survival" and "glmnet" R packages. The risk score for each patient was next calculated based on the expression levels of candidate genes and their corresponding coefficients in the optimal model with λ min. According to the median risk score, we then stratified the patients into high-risk (HR) and low-risk (LR) subgroups. Risk scores for patients in GSE2748 were calculated using the same formula for independent external validation. The differences in survival probabilities between HR and LR groups were identified by Kaplan-Meier survival analysis, and the prediction performances at 1, 3, and 5 years were evaluated by receiver operating characteristic (ROC) curves. In addition, we also investigated the po-

tential relationship between clinical characteristics and risk scores.

Biological functional analysis of HR versus LR

To explore biological differences between HR and LR subgroups, differential expression analysis was first performed under the threshold of | log2 (Fold change) | > 1 and adjusted $p < 0.05$. Differentially expressed genes (DEGs) were then analyzed using Gene Ontology (GO) and Kyoto Encyclopedia of Genes and Genomes (KEGG) enrichment analyses. Using the "GSVA" R package, we next computed gene set variation scores across the risk subgroups and identified risk score-related gene sets. In addition, we used the QuanTIseq algorithm to determine immune infiltration in subgroups. The immune cell compositions were eventually compared between risk subgroups.

Statistical analysis

Data analysis and plotting were executed using R software (version 4.2.1). To identify differences between groups, we used an independent-samples *t*-test on parametric continuous data and a Wilcoxon test on non-parametric continuous data. One-way ANOVA or non-parametric Kruskal-Wallis H-test was applied to the differences in the multi-groups. The Pearson test was employed to assess the correlation between the risk score and the gene set variation matrix. The overall survival was described by the Kaplan-Meier curve, and the log-rank test was used to calculate the significant difference of the survival probability. To evaluate the predictive performance of the risk signature, ROC curve analyses were conducted. The "clusterProfiler" R package was employed for GO and KEGG enrichment analyses, while the QuanTIseq algorithm was used for immune infiltration analysis. A p-value < 0.05 was considered statistically significant.

RESULTS

Differential expression and univariate Cox analysis of 17 CRGs

The workflow is shown in Figure 1. After excluding patients with incomplete clinical data and those with a survival time of less than 30 days, a total of 258 patients with PRCC from the TCGA cohort were ultimately enrolled. These patients were randomly divided into a training set (n = 183) and a validation set (n = 75). The clinical information of the patients in the TCGA cohort is shown in Table 1. There was no significant difference in clinical characteristics between the training and validation sets ($p > 0.05$). Under the criteria of | log2 (Fold change) | > 0.75 and adjusted p-value < 0.05, there were 8,041 DEGs between 258 PRCC tumor samples and 32 adjacent normal tissues in the TCGA cohort. Among 17 CRGs, only CDKN2A was upregulated, and 4 CRGs, including DBT, FDX1, SLC31A1, and ATP7A, were downregulated in tumors (Figure 2A). The expression patterns of 17 CRGs in PRCC and adjacent normal tissues are demonstrated in Figure 2B. Univariate Cox regression analysis of the 17 CRGs (Figure 2C) demonstrated that GLS and ATP7A were significant risk factors for the prognosis of PRCC (Hazard ratio > 1, $p < 0.05$). However, patients with high expression of DLST, PDHA1, PDHB, SLC25A3, and DLD had significantly improved overall survival (Hazard ratio < 1, $p < 0.05$).

Lasso-penalized Cox regression for 17 CRGs

Lasso-penalized Cox analysis (Figure 3A) identified 5 CRGs associated with overall survival in the training set, including DLST, PDHB, SLC25A3, ATP7A, and GLS. The risk score was calculated using the formula: risk score = [(-0.482130745) × expression of DLST] + [(-0.166984886) × expression of PDHB] + [(-0.113237601) × expression of SLC25A3] + [(0.01530986) × expression of ATP7A] + [(0.260613722) × expression of GLS]. As described in the methods section, patients in both training and validation sets were stratified into high-risk (HR) and low-risk (LR) subgroups (Figures 3B, 3C).

Kaplan-Meier survival analysis suggested that higher risk scores were associated with poorer overall survival in the training set (log-rank test, $p < 0.05$) (Figure 4A). This significant difference in overall survival between risk subgroups was also verified in the validation set (log-rank test, $p < 0.05$) (Figure 4B). To further verify the generalization performance of the risk signature, risk scores for each patient in GSE2748 were calculated using the aforementioned formula for external validation. Although not statistically significant, patients with high risk scores showed a trend toward lower survival (Figure 4C).

The ROC curves were used to evaluate the performance of the risk signature. As shown in Figures 4D - 4F, the area under the curve (AUC) values for the risk signature at 1, 3, and 5 years were all greater than 0.7 in the training, validation, and GSE2748 datasets, respectively.

No significant difference was observed in age distribution between risk subgroups ($p > 0.05$) (Figure 5A). Notably, in the training set alone, female patients had significantly higher risk scores than male patients ($p < 0.05$) (Figure 5A). Regarding AJCC stage, multiple comparison analysis indicated that PRCC patients with stage IV tended to have significantly higher risk scores than those with stage I ($p < 0.05$) (Figures 5A, 5B).

Biological functional analysis related to risk signature

To obtain a panoramic view of the biological functions associated with risk signature, differential expression analysis was performed between the LR and HR groups. GO enrichment analysis revealed that DEGs between the risk subgroups were mainly enriched in biological processes related to alpha-amino acid metabolic process, alanine metabolic process, pyruvate family amino acid metabolic process, and small molecule metabolic process (Figures 6A, 6B). KEGG pathway analysis fur-

Table 1. Clinical information of patients with PRCC from the TCGA cohort.

Characteristic	n	Training set	Validation set	Training vs. validation comparison, p
Total cases	258	183	75	
Gender				
Male	192 (74.4%)	135 (73.8%)	57 (76.0%)	0.709
Female	66 (25.6%)	48 (26.2%)	18 (24.0%)	
Age				
< 65	154 (59.7%)	113 (61.7%)	41 (54.7%)	0.292
≥ 65	104 (40.3%)	70 (38.3%)	34 (45.3%)	
Stage				
I	173 (67.1%)	122 (66.7%)	51 (68.0%)	0.979
II	22 (8.5%)	16 (8.7%)	6 (8.0%)	
III	47 (18.2%)	33 (18.0%)	14 (18.7%)	
IV	16 (6.2%)	12 (6.6%)	4 (5.3%)	

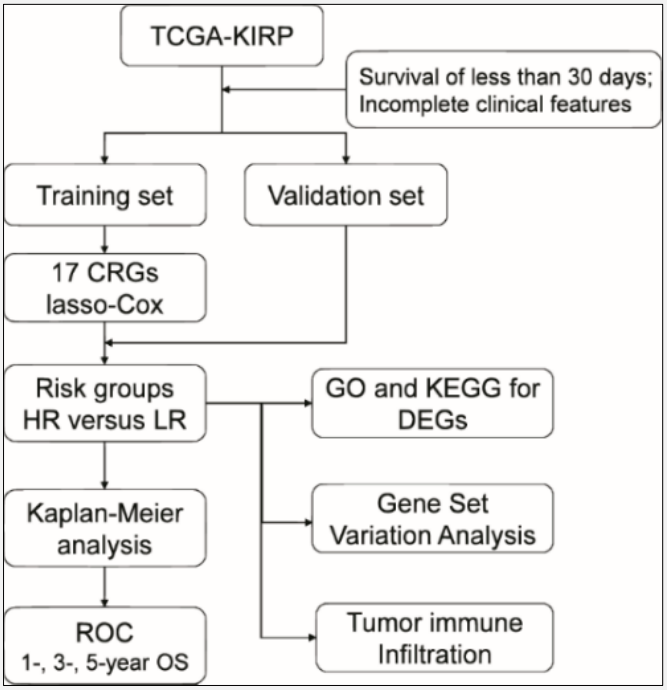

Figure 1. The workflow for risk signature establishment based on 17 CRGs.

ther identified significant differences in amino acid metabolism and carbohydrate metabolism pathways between the risk subgroups (Figures 6C, 6D). We further calculated gene set variation scores based on the expression profiles of the risk subgroups using GSVA. Correlation analysis between the gene set variation matrix and risk scores revealed that branched-chain amino acid metabolism, succinyl-CoA metabolism, and fatty acid metabolism were negatively correlated with risk scores (Figures 6E, 6F). To elucidate the tumor immune

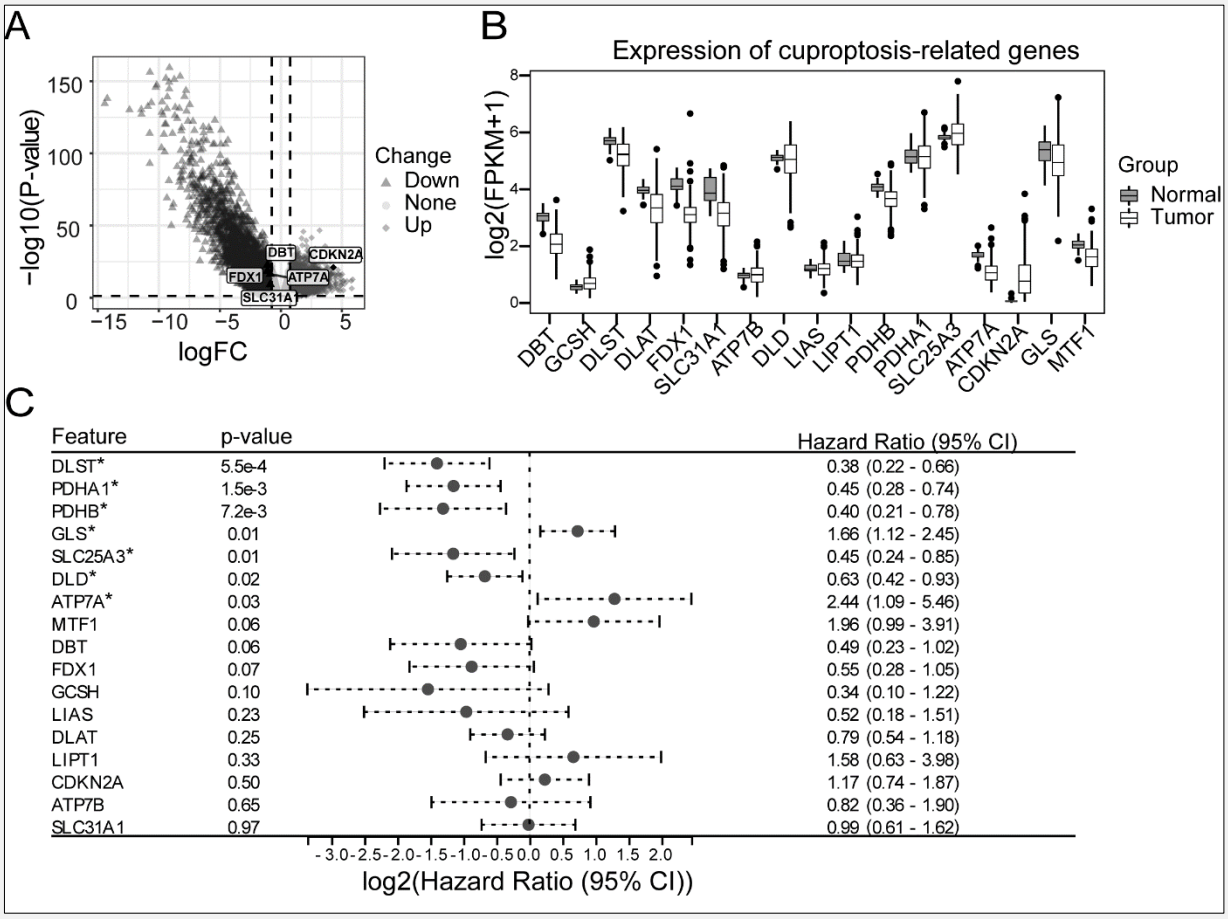

Figure 2. The expression and survival analysis of 17 CRGs.

A) The volcano plot for differential expression analysis between PRCC and adjacent normal tissues. The upregulated genes are marked with diamonds, while downregulated genes are marked with triangles under the criteria of | log2 (Fold change) | > 0.75 and p-value < 0.05. Five CRGs with significant change are annotated in volcano plot. B) The expression patterns of 17 CRGs in PRCC. C) The forest plot suggested univariate Cox analysis of 17 CRGs for overall survival in PRCC (* p < 0.05).

microenvironment related to the risk signature, infiltrating immune cell compositions in risk subgroups were identified using QuanTIseq algorithm. In PRCC, the predominant infiltrating cells were macrophages and neutrophils, followed by total lymphocytes with scattered myeloid dendritic cells (Figure 7A). Comparison between the LR and HR groups showed a slight but significant increase in M1 macrophages and regulatory T cells (Tregs) in the HR group ($p < 0.05$) (Figure 7B).

DISCUSSION

Cuproptosis is closely correlated to mitochondrial activity and mainly involves multiple processes, including reduction of copper ions, copper transportation, and lipoylation of tricarboxylic acid cycle components [11]. Although the mechanism is obscure, several studies have shown that the expression of CRGs was associated with the prognosis of tumors [14,15]. So far, the molecular pattern of CRGs in the PRCC has not been clearly defined. In this work, we identified the potential role of cuproptosis in the prognosis of PRCC and developed a CRG-related risk signature.

The expression levels of CRGs involved in the processes described above may determine the sensitivity of tu-

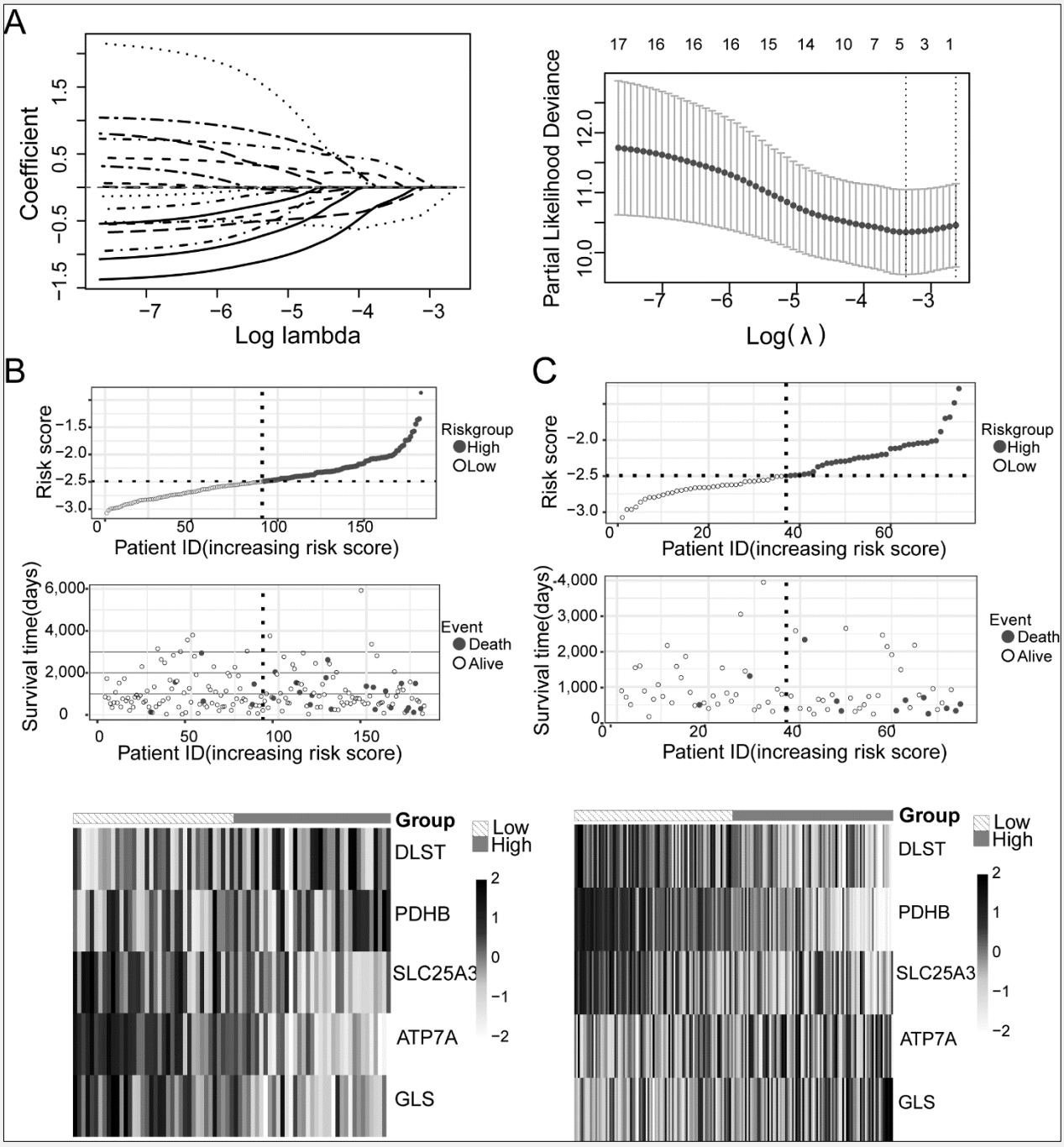

Figure 3. Risk signature establishment based on 17 CRGs.

A) Lasso-penalized Cox regression. The left part suggests the lasso coefficient profiles of 17 CRGs, and the curves with distinct line types indicate the change in the coefficient of variates included in model. The right part shows ten-fold cross-validation for optimal parameter selection in lasso model, and the vertical dotted lines represent the optimal log λ values through minimum and 1-SE criteria. B, C) The distribution of risk scores, survival status, and expression pattern of genes comprising the risk signature were shown in the training (B) and validation sets (C).

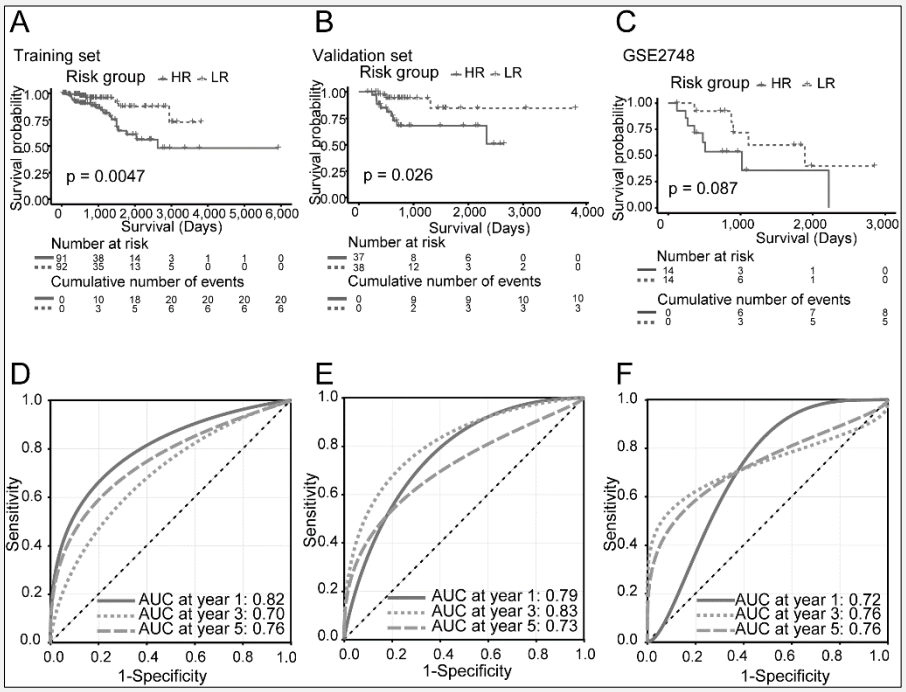

Figure 4. Survival analysis between risk subgroups in PRCC.

A - C) Kaplan-Meier survival analysis revealed that survival probabilities in HR group were lower than those of the LR group in training A) and validation sets B), Figure C suggests the survival curves in GSE2748 between HR and LR group for external validation. D - F) ROC curves at 1-, 3-, 5-year survival prediction are shown in training D), validation E), and GSE2748 F) datasets.

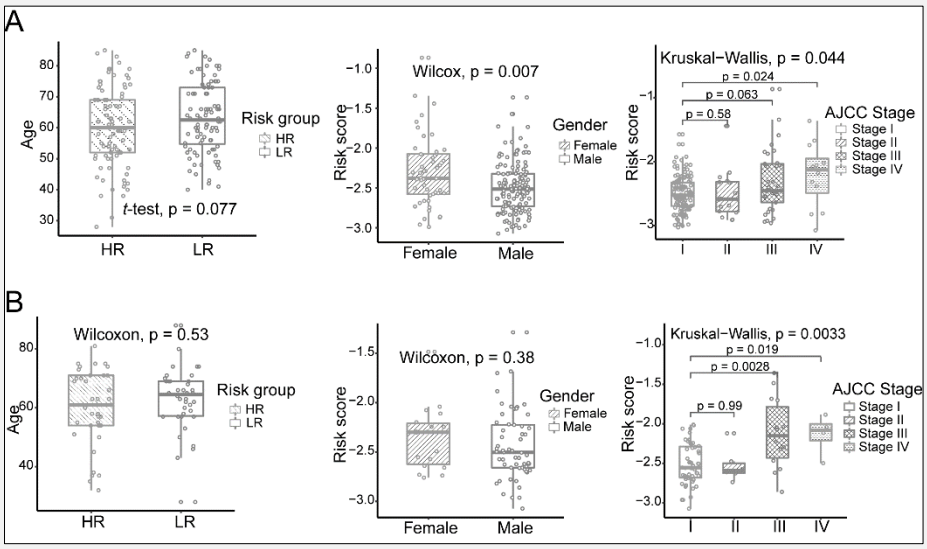

Figure 5. The relationship between risk scores and clinical characteristics.

A, B) Boxplots with hollow circles suggests that no difference was found in risk scores by age or gender, while risk scores in patients with stage IV were higher than those of patients with stage I in training A) and validation B) sets ($p < 0.05$).

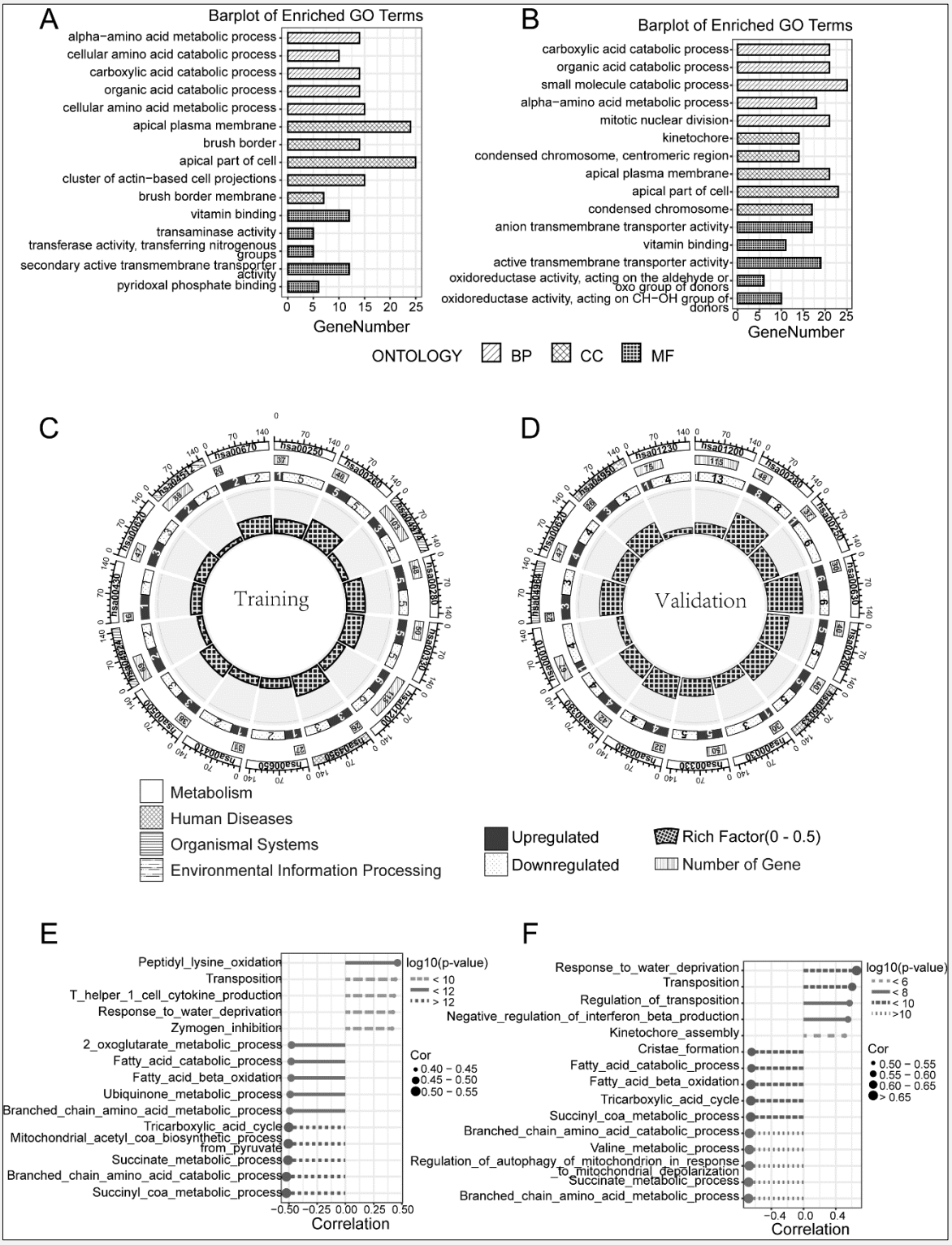

Figure 6. Biological function investigation.

A, B) GO enrichment analysis for differentially expressed genes by risk group in training A) and validation B) sets. C, D) KEGG analysis suggested that differentially expressed genes by risk group were mainly related to metabolism. E, F) Pearson´s correlation analysis of gene set variation with risk scores revealed that cellular metabolic processes were associated with risk scores in both the training set E) and the validation set F). The size of the lollipop indicates the strength of the correlation.

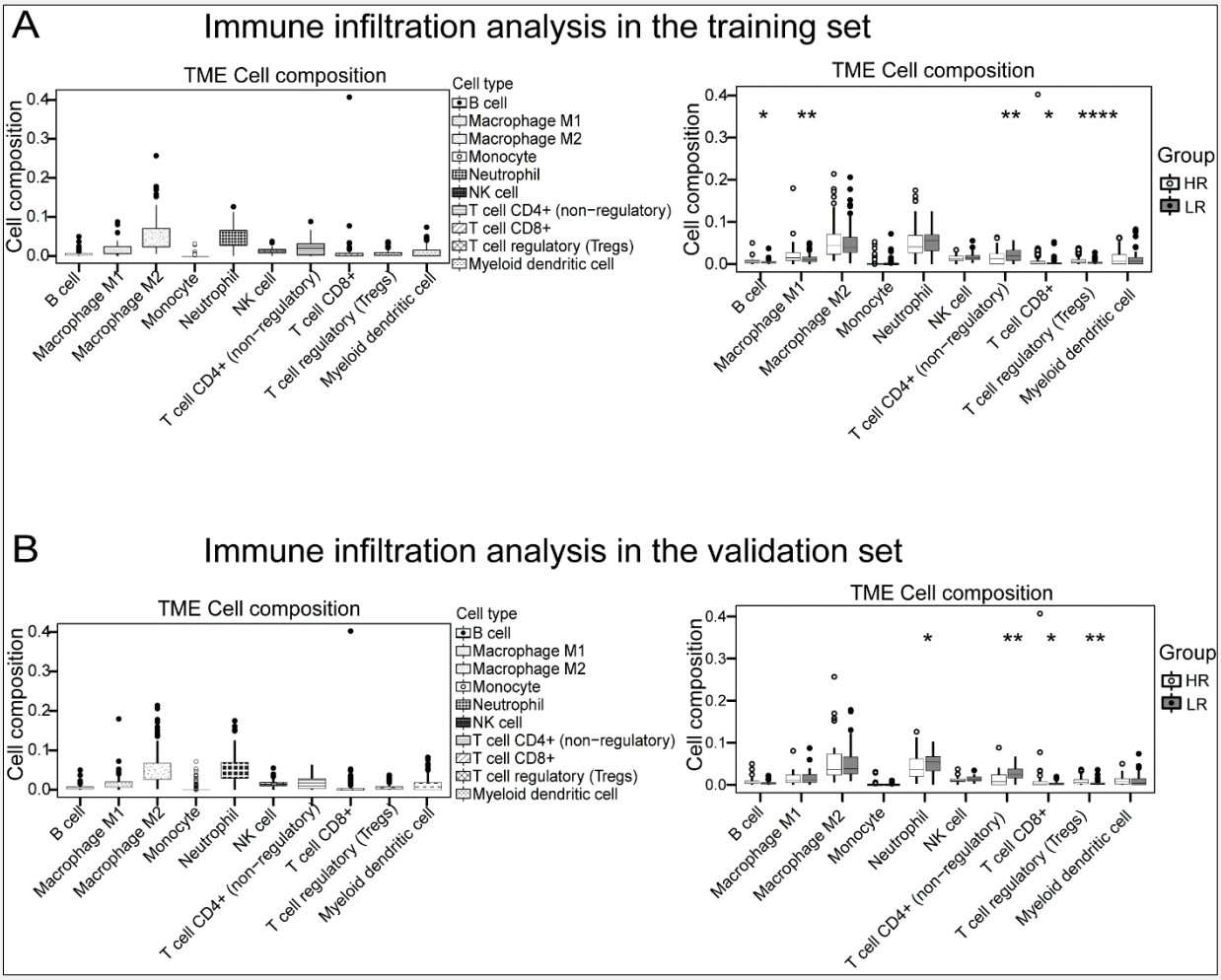

Figure 7. Immune infiltration analysis.

The compositions of ten different immune cell types were investigated using QuanTIseq method. Predominant infiltrating immune cells were macrophages and neutrophils, followed by total lymphocytes with scattered myeloid dendritic cells, and the Tregs were significantly higher around the HR tissues in both the training (A) and validation (B) sets (* $p < 0.05$, ** $p < 0.01$, *** $p < 0.001$, **** $p < 0.0001$).

mor cells to cuproptosis. Therefore, we first examined the expression pattern of the 17 CRGs. In the TCGA dataset, FDX1, SLC31A1, ATP7A, and DBT were all downregulated compared to normal tissues. FDX1 is a mitochondrial reductase which plays a crucial role in sterol hormone synthesis and mitochondrial metabolism [16]. FDX1 reduces the $Cu2^{+}$ to Cu^{+}, leading to increased cytotoxicity. The knockdown of FDX1 not only blocked cuproptosis, but also inhibited the lipoylation of DBT, GCSH, DLST, and DLAT, indicating that FDX1 represents a core element of cuproptosis [11]. Consistent with our results, one study has demonstrated that lower expression of FDX1 has been identified in most cancers and that it is strongly associated with a better prognosis in RCC [17]. Intriguingly, Zhang et al. found that the lower expression of FDX1 in HCC cells was associated with shorter survival time [15]. Although the knockdown of FDX1 reduced ATP production in lung cancer cells [18], the cell viability was not inhibited due to less additional ATP necessary for cell proliferation [19]. The mechanism by which FDX1 mediates cancer prognosis remains unclear. DBT (Dihydrothioctyl amine branched chain transacylase E2) could facilitate the formation of branched-chain keto acid dehydrogenase complex and participate in the metabolism of branched-chain amino acids. As is well-known to us, mutations of DBT lead to the maple syrup urine disease due to the accumulation of branched-chain

amino acids and keto acid derivatives [20]. Less attention has been focused, however, on the role of DBT in the tumorigenesis. One study has shown that DBT was less expressed in pancreatic cancer than in normal tissues and that it played a protective role in the prognosis [21]. Ko et al. found a positive correlation between DBT and the proto-oncogene BRAF and revealed that decreased expression of DBT in melanocytes inhibited activation of ERK/MAPK, p53, and apoptosis upon overexpression of BRAF V600E, a frequent oncogene mutation occurring in various cancers [22]. These findings hint that DBT may be related to cellular tolerance to oncogenes. SLC31A1 and ATP7A encode high-affinity copper transporters. Low expression of SLC31A1 induced copper depletion and led to subsequent activation of AMPK (AMP-activated protein kinase), which might reduce cell invasion [23]. CDKN2A is a tumor suppressor gene that encodes a protein involved in the cell cycle regulation and could induce cell cycle arrest in the G1/ G2 phase. Compared to adjacent normal tissues, CDKN2A is upregulated in most cancers [24], which was consistent with our study. One possibility is that the upregulation of CDKN2A in most cancers may act as a negative feedback mechanism to restrain tumor cell proliferation.

The tricarboxylic acid cycle provides intermediate products involved in several biological processes, particularly glutamine metabolism which supplies energy and fuel for cell growth [25]. More than that, the maintenance of the tricarboxylic acid cycle, which depended on the activation of the pyruvate dehydrogenase complex driven by AMPK, enabled cancer cells to adapt to the altered metabolic requirements during metastasis [26]. However, copper overload leads to the dysregulation of the tricarboxylic acid cycle by direct binding to its lipoylated components in cuproptosis. Based on these findings, we first performed the survival analysis of 17 CRGs in PRCC patients using univariate Cox regression. In this study, increased expression of DLST, PDHA1, PDHB, SLC25A3, or DLD was consistent with a better outcome, while higher expression of GLS or ATP7A tended to be associated with poorer prognosis in PRCC. In mitochondria, DLST plays a key role as an essential component of the α-ketoglutarate dehydrogenase complex responsible for the rate-limiting step of oxidative decarboxylation of α-ketoglutarate to succinyl-CoA. DLD, PDHA1, and PDHB together constitute the pyruvate dehydrogenase complex, which irreversibly catalyzes the decarboxylation of pyruvate to acetyl-CoA. The distinctive pattern of these vital enzymes indicated that patient outcomes were strongly correlated with cellular metabolic changes in tumor tissue.

A five-gene signature of CRGs including DLST, PDHB, GLS, ATP7A, and SLC25A3 was subsequently established using Lasso-penalized Cox regression in the training set. ROC curves suggested that AUCs for 1-, 3-, 5-year overall survival of the risk signature in the training set were 0.82, 0.70, and 0.76, respectively. The good predictive performance of the risk signature was also confirmed in the validation set. Meanwhile, we performed an external validation of the cuproptosis-related risk signature. In the GSE2748, we found that higher risk scores were associated with shorter survival time, although there was no significant difference between risk subgroups, which may have been caused by the small number of patients. The ROC curve suggested that AUCs for 1-, 3-, 5-year overall survival of the risk signature in GSE2748 were all larger than 0.7. In a meta cohort of PRCC, Zhang et al. summarized 13 CRGs and developed a risk signature based on the DEGs between cuproptosis-related subcluster [27]. The integration of the TCGA and GEO datasets expanded the sample size and thus increased the predictive performance of the risk signature [27]. Compared to the previous work, the merits of our work are the following: First, we collected more CRGs in our study and therefore displayed a more comprehensive and insightful expression pattern of CRGs in PRCC. In addition, we performed a regression analysis directly on the CRGs, which was more helpful to shed light on the relationship between cuproptosis and prognosis in PRCC patients. Finally, we also performed external validation to assess the generalizability of the predictive model, and the AUC values of the risk signature demonstrated better accuracy in distinguishing between low-risk and high-risk patients in both the TCGA and GEO datasets.

The expression of ATP7A and GLS was positively correlated with the risk score, whereas PDHB, DLST, and SLC25A3 were negatively correlated. ATP7A, the copper transporter ATPase, is expressed in various tissues, including intestine, kidney, brain, heart, and lung. Under the condition of copper overload, ATP7A can actively transfer copper out of the cells, thus attenuating copper-related cytotoxicity. Based on this evidence, targeting ATP7A in conjunction with retinoic therapy brings new insight for the treatment of neuroblastoma [28]. Additionally, studies have shown that ATP7A played a vital role in cell growth and metastasis, and downregulated ATP7A could inhibit phosphorylation of focal adhesion kinase and myeloid cell recruitment through the block of copper-dependent lysyl oxidase enzymes [29,30]. Therefore, the low expression of ATP7A may interfere with the natural processes of the metastatic microenvironment, thus resulting in a low risk of metastasis in PRCC. The SLC25 family consists of 53 members and is responsible for transportation of solutes across the inner mitochondrial membrane for many cellular processes [31]. Among those members, SLC25A3 plays a role in transferring phosphate to the mitochondrial matrix. The deletion of SLC25A3 resulted in a deficiency in mitochondrial ATP synthesis [32]. More than this, Boulet et al. found that the addition of copper to the culture medium was able to rescue cytochrome c oxidase deficiency caused by the complete deletion of SLC25A3 in HEK239 cells, suggesting an indispensable role for copper import of SLC25A3 [33]. In this risk signature, the complementary effects of SLC25A3 and ATP7A on copper transport implied that tumor

prognosis was strongly associated with copper metabolism in mitochondria. Glutaminase (GLS) catalyzes a rate-limiting step in the synthesis of glutamine, an essential amino acid critical for cellular energy and synthesis in cancer cells. However, as the tumor progresses, glutamine is transported from the tricarboxylic acid cycle to the nucleotide synthesis pathway in response to accelerated cell proliferation [34]. In the present study, expression of GLS was positively associated with risk scores in PRCC, suggesting that elevated glutamine metabolism was involved in driving tumor cell proliferation. In addition, glutathione derived from glutamine metabolism may inhibit cuproptosis by chelating copper even though cuproptosis is independent of oxidative stress [11]. Hereby, upregulated GLS in PRCC may indicate elevated glutamine metabolism and the enhanced resistance to cuproptosis in progressive tumors.

The relationships between risk scores and clinical characteristics were also analyzed. Our study suggests that patients with stage IV tend to exhibit higher risk scores in both training and validation sets. The consistency between the risk scores and tumor stages confirms the effectiveness of CRG-related risk signature for outcome prediction in PRCC. To explore the biological functions associated with the risk signature, we performed the differential expression analysis between risk subgroups. GO and KEGG analyses demonstrated that DEGs were associated with cellular amino acid metabolic processes and carbohydrate metabolism. Consistent with this, GSVA results indicated that the metabolism of branched-chain amino acids, succinyl-CoA, and the tricarboxylic acid cycle were closely correlated with risk scores. Metabolic alterations may promote tumor cells to adapt to the metastatic microenvironment and proliferate rapidly [25]. In PRCC, the immune infiltration analysis revealed that macrophages were the predominant infiltrating cells in tumor tissues, and the proportion of M2 macrophages was higher than that of M1 macrophages. It has long been known that the tumor microenvironment has a dual effect on tumor cells; it is capable of inhibiting or promoting tumor progression. The polarization of M2-type cells was primarily activated by the synergistic stimulation of various cytokines, including IL-4, IL-10, and TGF-β derived from T cells and tumor cells [35]. In turn, M2 macrophages could also promote tumor cell growth, angiogenesis, and immunosuppression by secreting a series of cytokines [35,36]. In this study, although very low in PRCC, the fraction of Tregs in HR was significantly higher than that in the LR subgroup. Many studies have suggested that infiltration of Tregs was associated with a poor tumor prognosis, which was consistent with the result of this study [37]. A potential mechanism of the poor outcome in PRCC may be the tumor escape promoted by Tregs through suppressing cytokines, inducing dendritic cell tolerance, and utilizing inhibitory receptors [38].

In summary, this study investigated the expression patterns of CRGs and developed a prognostic signature of CRGs in PRCC. This risk signature based on cuproptosis demonstrated a favorable performance for overall survival and was correlated with tumor immune infiltration and cellular metabolism. However, due to incomplete clinical information, factors such as hypertension and smoking were not included in this study to develop a prediction model for overall survival. Understanding the mechanism of cuproptosis and its potential effect on cellular metabolism may provide new insights into the progression of PRCC.

Declaration of Interest:

The authors have no conflicts of interest to declare.

References:

1. Znaor A, Lortet-Tieulent J, Laversanne M, Jemal A, Bray F. International variations and trends in renal cell carcinoma incidence and mortality. Eur Urol 2015 Mar;67(3):519-30. (PMID: 25449206)
2. Tippu Z, Au L, Turajlic S. Evolution of Renal Cell Carcinoma. Eur Urol Focus 2021 Jan;7(1):148-51. (PMID: 32007485)
3. Siegel RL, Miller KD, Jemal A. Cancer statistics, 2019. CA Cancer J Clin 2019 Jan;69(1):7-34. (PMID: 30620402)
4. Cancer Genome Atlas Research Network; Linehan WM, Spellman PT, et al. Comprehensive Molecular Characterization of Papillary Renal-Cell Carcinoma. N Engl J Med 2016 Jan 14; 374(2):135-45. (PMID: 26536169)
5. Akhtar M, Al-Bozom IA, Al Hussain T. Papillary Renal Cell Carcinoma (PRCC): An Update. Adv Anat Pathol 2019 Mar;26(2): 124-32. (PMID: 30507616)
6. Mendhiratta N, Muraki P, Sisk AE Jr, Shuch B. Papillary renal cell carcinoma: Review. Urol Oncol 2021 Jun;39(6):327-37. (PMID: 34034966)
7. Chandrasekar T, Klaassen Z, Goldberg H, Kulkarni GS, Hamilton RJ, Fleshner NE. Metastatic renal cell carcinoma: Patterns and predictors of metastases-A contemporary population-based series. Urol Oncol 2017 Nov;35(11):661.e7-661.e14. (PMID: 28728748)
8. Okazaki Y. The Role of Ferric Nitrilotriacetate in Renal Carcinogenesis and Cell Death: From Animal Models to Clinical Implications. Cancers (Basel) 2022 Mar 15;14(6):1495. (PMID: 35326646)
9. Wang Z, Song Q, Yang Z, Chen J, Shang J, Ju W. Construction of immune-related risk signature for renal papillary cell carcinoma. Cancer Med 2019 Jan;8(1):289-304. (PMID: 30516029)
10. Wang Y, Yan K, Lin J, et al. Three-gene risk model in papillary renal cell carcinoma: a robust likelihood-based survival analysis. Aging (Albany NY) 2020 Nov 5;12(21):21854-73. (PMID: 33154194)
11. Tsvetkov P, Coy S, Petrova B, et al. Copper induces cell death by targeting lipoylated TCA cycle proteins. Science 2022 Mar 18; 375(6586):1254-61. (PMID: 35298263)
12. Bian Z, Fan R, Xie L. A Novel Cuproptosis-Related Prognostic Gene Signature and Validation of Differential Expression in Clear Cell Renal Cell Carcinoma. Genes (Basel) 2022 May 10; 13(5):851. (PMID: 35627236)

13. Boulet A, Vest KE, Maynard MK, et al. The mammalian phosphate carrier SLC25A3 is a mitochondrial copper transporter required for cytochrome c oxidase biogenesis. J Biol Chem 2018 Feb 9;293(6):1887-96. (PMID: 29237729)

14. Lv H, Liu X, Zeng X, et al. Comprehensive Analysis of Cuproptosis-Related Genes in Immune Infiltration and Prognosis in Melanoma. Front Pharmacol 2022 Jun 28;13:930041. (PMID: 35837286)

15. Zhang Z, Zeng X, Wu Y, Liu Y, Zhang X, Song Z. Cuproptosis-Related Risk Score Predicts Prognosis and Characterizes the Tumor Microenvironment in Hepatocellular Carcinoma. Front Immunol 2022 Jul 11;13:925618. (PMID: 35898502)

16. Sheftel AD, Stehling O, Pierik AJ, et al. Humans possess two mitochondrial ferredoxins, Fdx1 and Fdx2, with distinct roles in steroidogenesis, heme, and Fe/S cluster biosynthesis. Proc Natl Acad Sci USA 2010 Jun 29;107(26):11775-80. (PMID: 20547883)

17. Zhang C, Zeng Y, Guo X, et al. Pan-cancer analyses confirmed the cuproptosis-related gene FDX1 as an immunotherapy predictor and prognostic biomarker. Front Genet 2022 Aug 5;13: 923737. (PMID: 35991547)

18. Zhang Z, Ma Y, Guo X, et al. FDX1 can Impact the Prognosis and Mediate the Metabolism of Lung Adenocarcinoma. Front Pharmacol 2021 Oct 8;12:749134. (PMID: 34690780)

19. Vander Heiden MG, Cantley LC, Thompson CB. Understanding the Warburg effect: the metabolic requirements of cell proliferation. Science 2009 May 22;324(5930):1029-33. (PMID: 19460998)

20. Pontoizeau C, Simon-Sola M, Gaborit C, et al. Neonatal gene therapy achieves sustained disease rescue of maple syrup urine disease in mice. Nat Commun 2022 Jun 7;13(1):3278. (PMID: 35672312)

21. Jiang Z, Zheng J, Liu J, Yang X, Chen K. Novel Branched-Chain Amino Acid-Catabolism Related Gene Signature for Overall Survival Prediction of Pancreatic Carcinoma. J Proteome Res 2022 Mar 4;21(3):740-6. (PMID: 34816714)

22. Ko T, Sharma R, Li S. Genome-wide screening identifies novel genes implicated in cellular sensitivity to BRAFV600E expression. Oncogene 2020 Jan;39(4):723-38. (PMID: 31548614)

23. Ramchandani D, Berisa M, Tavarez DA, et al. Copper depletion modulates mitochondrial oxidative phosphorylation to impair triple negative breast cancer metastasis. Nat Commun 2021 Dec 15;12(1):7311. (PMID: 34911956)

24. Kondapuram SK, Coumar MS. Pan-cancer gene expression analysis: Identification of deregulated autophagy genes and drugs to target them. Gene 2022 Nov 30;844:146821. (PMID: 35985410)

25. Vander Heiden MG, DeBerardinis RJ. Understanding the Intersections between Metabolism and Cancer Biology. Cell 2017 Feb 9;168(4):657-69. (PMID: 28187287)

26. Cai Z, Li CF, Han F, et al. Phosphorylation of PDHA by AMPK Drives TCA Cycle to Promote Cancer Metastasis. Mol Cell 2020 Oct 15;80(2):263-278.e7. (PMID: 33022274)

27. Zhang C, Huang R, Xi X. Cuproptosis patterns in papillary renal cell carcinoma are characterized by distinct tumor microenvironment infiltration landscapes. Front Mol Biosci 2022 Oct 5;9: 910928. (PMID: 36275614)

28. Cheung BB, Marshall GM. Targeting ATP7A to increase the sensitivity of neuroblastoma cells to retinoid therapy. Curr Cancer Drug Targets 2011 Sep;11(7):826-36. (PMID: 21762080)

29. Nagaraja GM, Othman M, Fox BP, et al. Gene expression signatures and biomarkers of noninvasive and invasive breast cancer cells: comprehensive profiles by representational difference analysis, microarrays and proteomics. Oncogene 2006 Apr 13;25(16): 2328-38. (PMID: 16314837)

30. Shanbhag V, Jasmer-McDonald K, Zhu S, et al. ATP7A delivers copper to the lysyl oxidase family of enzymes and promotes tumorigenesis and metastasis. Proc Natl Acad Sci USA 2019 Apr 2;116(14):6836-41. (PMID: 30890638)

31. Ruprecht JJ, Kunji ERS. The SLC25 Mitochondrial Carrier Family: Structure and Mechanism. Trends Biochem Sci 2020 Mar;45(3):244-58. (PMID: 31787485)

32. Asghari A, Marashi SA, Ansari-Pour N. A sperm-specific proteome-scale metabolic network model identifies non-glycolytic genes for energy deficiency in asthenozoospermia. Syst Biol Reprod Med 2017 Apr;63(2):100-12. (PMID: 28085499)

33. Cobine PA, Moore SA, Leary SC. Getting out what you put in: Copper in mitochondria and its impacts on human disease. Biochim Biophys Acta Mol Cell Res 2021 Jan;1868(1):118867. (PMID: 32979421)

34. Kodama M, Oshikawa K, Shimizu H, et al. A shift in glutamine nitrogen metabolism contributes to the malignant progression of cancer. Nat Commun 2020 Mar 17;11(1):1320. (PMID: 32184390)

35. Mantovani A, Sozzani S, Locati M, Allavena P, Sica A. Macrophage polarization: tumor-associated macrophages as a paradigm for polarized M2 mononuclear phagocytes. Trends Immunol 2002 Nov;23(11):549-55. (PMID: 12401408)

36. Rey-Giraud F, Hafner M, Ries CH. *In vitro* generation of monocyte-derived macrophages under serum-free conditions improves their tumor promoting functions. PLoS One 2012;7(8):e42656. (PMID: 22880072)

37. Seed RI, Kobayashi K, Ito S, et al. A tumor-specific mechanism of Treg enrichment mediated by the integrin αvβ8. Sci Immunol 2021 Mar 26;6(57):eabf0558. (PMID: 33771888)

38. Scott EN, Gocher AM, Workman CJ, Vignali DAA. Regulatory T Cells: Barriers of Immune Infiltration Into the Tumor Microenvironment. Front Immunol 2021 Jun 10;12:702726. (PMID: 34177968)